Tube-based robust MPC with adjustable uncertainty sets using zonotopes*

Vignesh Raghuraman and Justin P. Koeln

***Abstract*— A tube-based robust Model Predictive Control (MPC) formulation with adjustable uncertainty sets is presented where the size of the uncertainty set is optimized as part of the underlying optimization problem. To guarantee constraint satisfaction subject to uncertainties bounded to this set, Robust Positively Invariant (RPI) set computation and constraint tightening are integrated into the optimization problem. Zonotopes are used to represent the set containment conditions that define RPI sets and constraint tightening as linear constraints. The Hausdorff distance metric is shown to reduce conservatism when optimizing the size of these tightened constraint sets. Finally, a numerical example demonstrates the ability to optimize the size of the uncertainty set within a robust MPC formulation and highlights the benefits and limitations of this approach.**

I. INTRODUCTION

Model Predictive Control (MPC) is widely used for the control of constrained systems where state and input constraints are explicitly embedded in the optimization problem. For the control of systems with unknown but bounded additive disturbances, there exists many different robust MPC formulations designed to guarantee robust state and input constraint satisfaction in the presence of these uncertainties [1], [2]. In these formulations, the bounded disturbances are typically restricted to a uncertainty set of predetermined shape and size.

A specific form of robust MPC known as *tube-based* robust MPC is widely used to provide robustness with only a slight increase in computational complexity [3], [4]. Tubes bound the true system trajectories within a neighborhood centered around nominal state and input trajectories optimized by the robust MPC controller. The sizes of these tubes depend on the size of the bounded uncertainty set and are typically computed using a Robust Positively Invariant (RPI) set. This RPI set is then used to tighten the state and input constraint sets such that if nominal trajectories satisfy the tightened constraints, then the true system trajectories are guaranteed to satisfy the original constraints. Typically, the size of the uncertainty set is known *a priori* and both the RPI set and the constraint tightening are computed offline.

Recently, there has been a growing interest to compute the uncertainty set as a part of the robust MPC optimization problem and these problems are referred to as robust MPC with adjustable uncertainty sets (RMPC-AU) [5], [6]. Applications that can benefit from RMPC-AU formulation include economic reserve capacity optimization [7], robust input tracking [8], [9], distributed MPC [10], and hierarchical MPC [11]. In the reserve capacity problem, the adjustable uncertainty set is characterized as a reserve capacity which can be provided by an operator to third-parties for some monetary benefits without violating it's own operational constraints [7]. While in robust input tracking from [8] and [9], the adjustable uncertainty set is quantified as the largest input set that can be tracked without violating the system constraints. In these applications, maximization of uncertainty sets is desired.

However, in distributed MPC, where the coupling between neighboring subsystems is treated as a bounded disturbance, minimizing the size of disturbance sets provides reduced conservatism and improved performance [10]. Finally, in hierarchical MPC, differences between control decisions by controllers at different levels of the hierarchy can be viewed as bounded disturbances [11]. In this case, the optimal size of bounding sets is to be determined while solving the upper-level optimization problem to provide a time-varying optimal balance between performance at the upper-level and flexibility at the lower-level.

In the RMPC-AU design from [5] and [6], the adjustable uncertainty sets are defined as the affine transformation of an *a priori* chosen convex primitive set in the form of ellipsoids, hyper-rectangles, or polytopes. Thus, the shape and size of these uncertainty sets are optimized by determining these affine transformation variables from the feasible domain set.

Specifically in [5], control policies are optimized from a chosen class of piece-wise affine policy functions to achieve computational tractability and feasibility for a finite horizon operation. This work is extended to an infinite horizon operation in [6] by enforcing a terminal constraint set, which is an inner-approximation of the positive invariant terminal set computed based on the chosen primitive set. Moreover, when norm-balls are used to represent these uncertainty sets, as in [5], the underlying optimization requires solving a semi-definite program which could pose computational challenges with increase in system dimension and complexity of the primitive set. Similarly in [6], the construction of robust precursor set through repetitive intersections particularly for a long prediction horizon is likely to result in large number of inequalities using H-Rep which adds complexity to the underlying optimization problem. Additionally, both [5] and [6] use a min-max optimization approach for dealing with uncertainty which is generally more computationally complex than tube-based robust MPC [12].

*This material is based upon work supported by the National Science Foundation under Grant No. 1849500.

The authors are with the Department of Mechanical Engineering, The University of Texas at Dallas, 800 W. Campbell Rd, Richardson, TX, USA. Email: vignesh.raghuraman@utdallas.edu, justin.koeln@utdallas.edu.

Specifically with regards to tube-based robust MPC, RPI sets are traditionally computed offline using the iterative procedure from [13] in H-Rep which is an outer-approximation of the minimal RPI (mRPI) set [14]. To improve computational performance and scalability, one-step optimization-based techniques have been developed in [15]. To further improve computational performance, similar one-step approaches using *zonotopes* with a corresponding Generator-Representation (G-Rep) have been developed in [16] for computing both outer-approximations of the mRPI set and inner-approximations of the Pontryagin (Minkowski) difference used for constraint tightening. In both cases, set computations are based on set containment conditions which can be reformulated as linear constraints using the techniques in [17].

This paper leverages the recent developments in one-step RPI and Pontryagin difference set computations to embed the computation of these sets within a robust tube-based MPC formulation that simultaneously optimizes nominal state and input trajectories along with the size of the uncertainty set. In addition to presenting this novel tube-based MPC formulation, this paper shows how all of the set containment constraints of robust MPC can be imposed as linear constraints and how the formulation of the cost function plays a critical role in minimizing conservatism introduced through inner- and outer-approximations of these sets.

The remainder of the paper is organized as follows. Section II introduces the notation used throughout the paper. Section III provides a review of robust tube-based MPC, while Section IV presents the proposed MPC formulation with uncertainty set size optimization and integrated RPI and tightened constraint set computations. Section V introduces zonotopes and the zonotope-based set containment conditions required to recast the robust MPC containment constraints as linear constraints, as discussed in Section VI. Finally, Section VII presents a numerical example to demonstrate the key features and limitations of including uncertainty set sizing within a robust MPC optimization while Section VIII summarizes the conclusions of the paper.

II. NOTATION AND PRELIMINARIES

For a discrete time system, the notation $\mathbf{x}(k)$ denotes the state $\mathbf{x}$ at time step k. The brace notation $j \in \{k, \cdots, k+N-1\}$ denotes all integers from k to until $k+N-1$. For MPC, the double-index notation $\hat{\mathbf{x}}(k+j|k)$ denotes the predicted state $\hat{\mathbf{x}}$ at future time step $k+j$ determined at k. For notational convenience, vectors and matrices are bolded and sets are shown in caligraphic font. The weighted norm is defined as $||\mathbf{x}||^2_{\mathbf{Q}} = \mathbf{x}^\top \mathbf{Q}\mathbf{x}$ where $\mathbf{Q}$ is a positive definite diagonal weighting matrix. A vector of ones of appropriate dimension is given by $\mathbf{1}$. For a matrix $\mathbf{A}$, $|\mathbf{A}|$ denotes the element-wise absolute value. The notation $||\cdot||_p$ denotes the $p-$norm of a vector. The sets $\mathbb{N}_+$ and $\mathbb{R}_+$ denote the set of natural numbers and positive real numbers, respectively. For sets $\mathcal{X}, \mathcal{Y} \subset \mathbb{R}^n$, $\mathcal{X} \oplus \mathcal{Y}$ denotes the Minkowski sum and $\mathcal{X} \ominus \mathcal{Y}$ denotes the Pontryagin/Minkowski difference of $\mathcal{Y}$ from $\mathcal{X}$. The volume ratio of $\mathcal{X}$ with respect to $\mathcal{Y}$ is given by $V_r = \left(\frac{V(\mathcal{X})}{V(\mathcal{Y})}\right)^{\frac{1}{n}}$ where $V(\cdot)$ denotes the volume of a set. The convex polytope $\mathcal{S} \subset \mathbb{R}^n$ in H-Rep is defined as $\mathcal{S} = \{\mathbf{s} \in \mathbb{R}^n \mid \mathbf{F}\mathbf{s} \leq \mathbf{h}\}$ such that $\mathbf{F} \in \mathbb{R}^{n_h \times n}$ and $\mathbf{h} \in \mathbb{R}^{n_h}$ where n_h denotes the number of halfspaces. A zonotope $\mathcal{Z} = \{\mathbf{G}, \mathbf{c}\} \subset \mathbb{R}^n$ defined by $\mathcal{Z} = \{\mathbf{G}\boldsymbol{\xi} + \mathbf{c} \mid ||\boldsymbol{\xi}||_\infty \leq 1\}$, where n_g denotes the number of generators such that $\mathbf{G} \in \mathbb{R}^{n \times n_g}$ and $\mathbf{c} \in \mathbb{R}^n$. For zonotopes $\mathcal{X} = \{G_x, c_x\} \subset \mathbb{R}^n, \mathcal{Y} = \{G_y, c_y\} \subset \mathbb{R}^n$, the linear transformation by a matrix $\mathbf{R} \in \mathbb{R}^{m \times n}$ is defined as $\mathbf{R}\mathcal{X} = \{\mathbf{R}\mathbf{G}_x, \mathbf{R}\mathbf{c}_x\}$ and the Minkowski sum $\mathcal{X} \oplus \mathcal{Y} = \left\{\begin{bmatrix}\mathbf{G}_x & \mathbf{G}_y\end{bmatrix}, \mathbf{c}_x + \mathbf{c}_y\right\}$. A hypercube with edge length d is denoted $d\mathcal{B}$, where $\mathcal{B}$ is the unit hypercube defined by $\mathcal{B} = \{b \mid ||b||_\infty \leq 1\}$.

III. ROBUST MPC BACKGROUND

Consider the discrete linear time-invariant system

$$\mathbf{x}(k+1) = \mathbf{A}\mathbf{x}(k) + \mathbf{B}\mathbf{u}(k) + \mathbf{w}(k), \tag{1}$$

where $\mathbf{x} \in \mathbb{R}^n$ are the states, $\mathbf{u} \in \mathbb{R}^m$ are the inputs, and $\mathbf{w} \in \mathbb{R}^n$ are the additive disturbances. It is assumed that the pair $(\mathbf{A}, \mathbf{B})$ is stabilizable. The states, inputs, and disturbances are subject to the constraints

$$\mathbf{x}(k) \in \mathcal{X}, \quad \mathbf{u}(k) \in \mathcal{U}, \quad \mathbf{w}(k) \in \mathcal{W}, \tag{2}$$

assuming $\mathcal{X}$, $\mathcal{U}$, and $\mathcal{W}$ are compact and convex polytopes containing the origin in their interiors.

The widely-used tube-based robust MPC from [4] solves the following constrained optimization problem at every time step $k \geq 0$,

$$J^*(\mathbf{x}(k)) = \min_{\hat{\mathbf{x}}(k|k),\, \hat{\mathbf{U}}(k)} \sum_{j=k}^{k+N-1} \ell(j|k) + \ell_f(k+N|k), \tag{3a}$$

$$\text{s.t.} \quad \forall j \in [k, k+N-1],$$

$$\hat{\mathbf{x}}(j+1|k) = \mathbf{A}\hat{\mathbf{x}}(j|k) + \mathbf{B}\hat{\mathbf{u}}(j|k), \tag{3b}$$

$$\hat{\mathbf{x}}(j|k) \in \hat{\mathcal{X}} \triangleq \mathcal{X} \ominus \mathcal{E}, \tag{3c}$$

$$\hat{\mathbf{u}}(j|k) \in \hat{\mathcal{U}} \triangleq \mathcal{U} \ominus K\mathcal{E}, \tag{3d}$$

$$\mathbf{x}(k) - \hat{\mathbf{x}}(k|k) \in \mathcal{E}, \tag{3e}$$

$$\hat{\mathbf{x}}(k+N|k) \in \hat{\mathcal{T}}. \tag{3f}$$

This MPC formulation has a prediction horizon of N steps and optimizes $\hat{\mathbf{U}}(k) \triangleq \{\hat{\mathbf{u}}(j|k)\}_{j=k}^{k+N-1}$ to minimize the cost function (3a) which is typically formulated with stage costs $\ell(j|k) = \|\hat{\mathbf{x}}(j|k)\|^2_{\mathbf{Q}} + \|\hat{\mathbf{u}}(j|k)\|^2_{\mathbf{R}}$ and terminal cost $\ell_f(k+N|k) = \|\hat{\mathbf{x}}(k+N|k)\|^2_{\mathbf{P}}$, where $\mathbf{Q}$ and $\mathbf{R}$ are design parameters and $\mathbf{P}$ satisfies the discrete-time algebraic Riccati equation. First introduced in [4], this tube-based robust MPC formulation also allows the initial nominal state $\hat{\mathbf{x}}(k|k)$ to be a decision variable.

Based on the solution to (3), the control input applied to (1) is

$$\mathbf{u}(k) = \hat{\mathbf{u}}^*(k|k) + \mathbf{K}\left(\mathbf{x}(k) - \hat{\mathbf{x}}^*(k|k)\right), \tag{4}$$

where $\hat{\mathbf{x}}^*(k|k)$ and $\hat{\mathbf{u}}^*(k|k)$ denote the optimal state and input at time step k and $\mathbf{K}$ is a stabilizing feedback control law, often chosen as the infinite-horizon, discrete-time LQR

controller. This stabilizing control law ensures that the difference, $\mathbf{x}(k) - \hat{\mathbf{x}}(k|k)$, between the true and nominal state trajectories satisfying (1) and (3b) respectively, always stays within a bounded set, $\mathcal{E}$, given the bounded disturbances, $\mathbf{w}(k) \in \mathcal{W}$.

This bounding set, $\mathcal{E}$, is typically computed as an outer-approximation of the mRPI set satisfying

$$\mathbf{A_K}\mathcal{E} \oplus \mathcal{W} \subseteq \mathcal{E}, \tag{5}$$

where $\mathbf{A_K} = \mathbf{A} + \mathbf{BK}$. Thus, if the nominal state starts off close to the true state, as enforced by (3e), then the difference between the two state trajectories will always remain within $\mathcal{E}$. This enables the constraint tightening approach used in (3c) and (3d), where if the nominal trajectories satisfy the tightened constraints, the true trajectories will satisfy the original state and input constraints from (2).

The terminal set $\hat{\mathcal{T}}$ in (3f) is typically included to guarantee robust stability by choosing $\hat{\mathcal{T}}$ such that

$$\mathbf{A_K}\hat{\mathcal{T}} \subseteq \hat{\mathcal{T}}, \quad \hat{\mathcal{T}} \subseteq \hat{\mathcal{X}}, \quad \mathbf{K}\hat{\mathcal{T}} \subseteq \hat{\mathcal{U}}. \tag{6}$$

Traditionally, tube-based robust MPC development starts with the offline processes of: 1) determining the uncertainty bounding set, $\mathcal{W}$; 2) computing an outer-approximation of the mRPI set, $\mathcal{E}$; and 3) computing the tightened constraint sets $\hat{\mathcal{X}}, \hat{\mathcal{U}}$, and $\hat{\mathcal{T}}$. The online process then consists of solving (3) and applying the input defined in (4).

However, there is growing interest in developing MPC-based control strategies [5], [6] where the size of the uncertainty set, $\mathcal{W}$, is included in the optimization. This prohibits the offline computation of the mRPI sets and constraint tightening which are usually time-consuming calculations that scale poorly with the number of states and inputs.

Therefore, this paper presents a scalable robust MPC approach where the size of $\mathcal{W}$, and the corresponding sizes of $\mathcal{E}$, $\hat{\mathcal{X}}$, $\hat{\mathcal{U}}$, and $\hat{\mathcal{T}}$, are all computed online as part of the overall optimization problem.

IV. Robust MPC with Integrated RPI Set Computation and Constraint Tightening

This paper assumes that the shape of the uncertainty set is predetermined but the size is variable such that

$$\mathbf{w}(k) \in \mathcal{W}(\mathbf{\Phi}_w), \tag{7}$$

where $\mathbf{\Phi}_w$ is a scaling variable with positive entries. Similar scaling variables have been used in [10] and [18]. In [10], a scaling variable $\mathbf{\Phi}_f$ is used to scale the offset vector of the uncertainty set represented in H-Rep as

$$\mathcal{W}(\mathbf{\Phi}_f) = \{\mathbf{w} \mid \mathbf{Hw} \leq \mathbf{\Phi}_f\},\ \mathbf{\Phi}_f \in \mathbb{R}^{n_h}. \tag{8}$$

Alternatively, in [18], the scaling variable Φ_m scales the magnitude of a nominal uncertainty set $\mathcal{W}^*$ where

$$\mathcal{W}(\Phi_m) = \Phi_m \mathcal{W}^*,\ \Phi_m \in \mathbb{R}_+. \tag{9}$$

Since the scaling variable $\mathbf{\Phi}_w$ in (7) is a decision variable, the sets $\mathcal{E}$, $\hat{\mathcal{X}}$, $\hat{\mathcal{U}}$, and $\hat{\mathcal{T}}$ cannot be precomputed. Instead, each of these sets will have a nominal shape and a corresponding scaling variable such that

$$\mathcal{E} \subseteq \tilde{\mathcal{E}}(\mathbf{\Phi}_\varepsilon),\ \tilde{\mathcal{X}}(\mathbf{\Phi}_x) \subseteq \hat{\mathcal{X}},\ \tilde{\mathcal{U}}(\mathbf{\Phi}_u) \subseteq \hat{\mathcal{U}},\ \tilde{\mathcal{T}}(\mathbf{\Phi}_t) \subseteq \hat{\mathcal{T}}. \tag{10}$$

With the inclusion of these scalable sets, (3) is reformulated as

$$J^*(\mathbf{x}(k)) = \min_{\substack{\mathbf{\Phi},\, \hat{\mathbf{x}}(k|k),\\ \hat{\mathbf{U}}(k)}} \sum_{j=k}^{k+N-1} \ell(j|k) + \ell_f(k+N|k) + \ell_{\mathbf{\Phi}}, \tag{11a}$$

$$\text{s.t.} \quad \forall j \in [k, k+N-1]\,,$$

$$\hat{\mathbf{x}}(j+1|k) = \mathbf{A}\hat{\mathbf{x}}(j|k) + \mathbf{B}\hat{\mathbf{u}}(j|k), \tag{11b}$$

$$\hat{\mathbf{x}}(j|k) \in \tilde{\mathcal{X}}(\mathbf{\Phi}_x), \qquad \tilde{\mathcal{X}}(\mathbf{\Phi}_x) \oplus \tilde{\mathcal{E}}(\mathbf{\Phi}_\varepsilon) \subseteq \mathcal{X}, \tag{11c}$$

$$\hat{\mathbf{u}}(j|k) \in \tilde{\mathcal{U}}(\mathbf{\Phi}_u), \qquad \tilde{\mathcal{U}}(\mathbf{\Phi}_u) \oplus \mathbf{K}\tilde{\mathcal{E}}(\mathbf{\Phi}_\varepsilon) \subseteq \mathcal{U}, \tag{11d}$$

$$\mathbf{x}(k) - \hat{\mathbf{x}}(k|k) \in \tilde{\mathcal{E}}(\mathbf{\Phi}_\varepsilon), \tag{11e}$$

$$\mathbf{A_K}\tilde{\mathcal{E}}(\mathbf{\Phi}_\varepsilon) \oplus \mathcal{W}(\mathbf{\Phi}_w) \subseteq \tilde{\mathcal{E}}(\mathbf{\Phi}_\varepsilon), \tag{11f}$$

$$\hat{\mathbf{x}}(k+N|k) \in \tilde{\mathcal{T}}(\mathbf{\Phi}_t), \qquad \mathbf{A_K}\tilde{\mathcal{T}}(\mathbf{\Phi}_t) \subseteq \tilde{\mathcal{T}}(\mathbf{\Phi}_t), \tag{11g}$$

$$\tilde{\mathcal{T}}(\mathbf{\Phi}_t) \subseteq \tilde{\mathcal{X}}(\mathbf{\Phi}_x), \qquad \mathbf{K}\tilde{\mathcal{T}}(\mathbf{\Phi}_t) \subseteq \tilde{\mathcal{U}}(\mathbf{\Phi}_u). \tag{11h}$$

By allowing the RPI and tightened constraint sets to vary in size, the scaling matrices $\mathbf{\Phi} = \{\mathbf{\Phi}_w, \mathbf{\Phi}_\varepsilon, \mathbf{\Phi}_x, \mathbf{\Phi}_u, \mathbf{\Phi}_t\}$ are included as decision variables in (11). The sizes of these corresponding sets are prioritized in (11a) using a generic cost function $\ell_{\mathbf{\Phi}} = \ell_{\mathbf{\Phi}}(\mathbf{\Phi}_w, \mathbf{\Phi}_\varepsilon, \mathbf{\Phi}_x, \mathbf{\Phi}_u, \mathbf{\Phi}_t)$ as discussed in more detail in Section VIB. The set containment condition in (11c) has been added to ensure that

$$\tilde{\mathcal{X}}(\mathbf{\Phi}_x) \subseteq \mathcal{X} \ominus \tilde{\mathcal{E}}(\mathbf{\Phi}_\varepsilon) \subseteq \hat{\mathcal{X}} \triangleq \mathcal{X} \ominus \mathcal{E}, \tag{12}$$

is satisfied based on the extensive property of the closing of $\tilde{\mathcal{X}}(\mathbf{\Phi}_x)$ by $\tilde{\mathcal{E}}(\mathbf{\Phi}_\varepsilon)$. A similar set containment condition has been added for the input set in (11d) to ensure satisfaction of

$$\tilde{\mathcal{U}}(\mathbf{\Phi}_u) \subseteq \mathcal{U} \ominus \mathbf{K}\tilde{\mathcal{E}}(\mathbf{\Phi}_\varepsilon) \subseteq \hat{\mathcal{U}} \triangleq \mathcal{U} \ominus \mathbf{K}\mathcal{E}. \tag{13}$$

The set containment condition in (11f) has been added to ensure that $\tilde{\mathcal{E}}(\mathbf{\Phi}_\varepsilon)$ satisfies the definition of an RPI set from (5). Finally, the set containment conditions in (11g) and (11h) have been added to ensure that $\tilde{\mathcal{T}}(\mathbf{\Phi}_t)$ satisfies the properties of a terminal set from (6). Note that the size of the uncertainty set, determined by the scaling matrix $\mathbf{\Phi}_w$, only appears in (11f) but directly affects the size of the RPI set and the state, input, and terminal set constraint tightening. The following theorem mathematically proves the recursive feasibility of the proposed tube-based robust MPC framework.

Theorem 1: If the MPC optimization problem in (11) is feasible at time step k, then it is feasible at time step $k+1$.

Proof: The proof is the same as that of tube-based robust MPC from Proposition 3 in [4] with the addition that the candidate solution for the scaling variables at time step $k+1$ is equal to the optimal solution from time step k such that $\mathbf{\Phi}(k+1) = \mathbf{\Phi}^*(k)$. ■

Usually, in constrained robust MPC, desired performance is achieved by letting the state and input trajectories operate

close to the bounds of the tightened state and input constraints. A typical example is the thermal management of aircraft electro-thermal systems where the temperatures of the system components are allowed to approach the respective upper-bounds to minimize coolant flow and achieve energy-efficient operation [19]. Usually, the larger the uncertainty set, the smaller the tightened state, input, and terminal sets, which results in loss of desired system performance. Thus, there exists a trade-off between the size of the uncertainty set and system performance, which must be optimized.

The main contribution of this paper lies in showing that despite the introduction of scaling variables, $\mathbf{\Phi}$, as decision variables, all of the point and set containment conditions in (11c)-(11h) can be represented as linear constraints. Therefore, if (3) is formulated as a Quadratic Program (QP), then (11) is also a QP. This key feature of the proposed approach is enabled through the use of *zonotopes*.

V. Background on Zonotopes and Zonotopic Set Operations

A zonotope is the Minkowski sum of a finite set of line segments or, equivalently, the image of a hypercube under an affine transformation [20], [21]. Using G-Rep, a zonotope $\mathcal{Z} \subset \mathbb{R}^n$ is defined by its center $\mathbf{c} \in \mathbb{R}^n$ and n_g generators $\mathbf{g}_i$ that form the columns of $\mathbf{G} \in \mathbb{R}^{n \times n_g}$, such that $\mathcal{Z} = \{\mathbf{G}\boldsymbol{\xi} + \mathbf{c} \mid \|\boldsymbol{\xi}\|_\infty \leq 1\}$. The complexity of a zonotope is captured by its order, $o = \frac{n_g}{n}$.

Zonotopes have been widely used due to their computational efficiency in reach set calculations for hybrid system verification, estimation, and MPC [22]–[25]. As with the iterative algorithm in [26], computing these reach sets utilizes linear transformation and Minkowski sum operations. Zonotopes are closed under these operations (i.e. the Minkowski sum of two zonotopes is a zonotope) and the number of generators grows linearly with the number of Minkowski sum operations, compared to the potential exponential growth with H-Rep. The results in this paper heavily rely on the following zonotope containment condition from [17].

Lemma 1: (Corollary 4 of [17]) Given two zonotopes $\mathcal{F} = \{\mathbf{G}_f, \mathbf{c}_f\} \subset \mathbb{R}^n$ and $\mathcal{H} = \{\mathbf{G}_h, \mathbf{c}_h\} \subset \mathbb{R}^n$, $\mathcal{F} \subseteq \mathcal{H}$ if there exists $\mathbf{\Gamma} \in \mathbb{R}^{n_h \times n_f}$ and $\boldsymbol{\beta} \in \mathbb{R}^{n_h}$ such that

$$\mathbf{G}_f = \mathbf{G}_h\mathbf{\Gamma}, \quad \mathbf{c}_h - \mathbf{c}_f = \mathbf{G}_h\boldsymbol{\beta}, \quad |\mathbf{\Gamma}|\mathbf{1} + |\boldsymbol{\beta}| \leq \mathbf{1}. \quad (14)$$

Using this zonotope containment condition, the main idea is to scale a zonotope such that set containment conditions from (11c) and (11d) and RPI set condition from (11f) holds.

Definition 1: The zonotope $\mathcal{Z}(\mathbf{\Phi}) = \{\mathbf{G}\mathbf{\Phi}, \mathbf{c}\} \subset \mathbb{R}^n$ is a scaled version of the nominal zonotope $\mathcal{Z} = \{\mathbf{G}, \mathbf{c}\}$ with the generator matrix $\mathbf{G}$ scaled by a diagonal matrix $\mathbf{\Phi} \in \mathbb{R}^{n_g \times n_g}, \mathbf{\Phi} = \text{diag}(\phi_i), \phi_i > 0, \forall i \in \{1, \cdots, n_g\}$.

Assumption 1: For the chosen $\mathbf{G}$ and the system $(\mathbf{A_K}, \mathcal{W})$, there exists a $\mathbf{\Phi} \in \mathbb{R}^{n_g \times n_g}$ that scales the RPI set $\mathcal{E}$ such that (5) holds.

While *Assumption 1* is needed to exclude certain systems that do not admit RPI sets [15], this assumption is typically mild in practice through the proper choice of $\mathbf{G}$, as discussed below.

Theorem 2: (Theorem 6 of [16]) The zonotope $\mathcal{Z}(\mathbf{\Phi}) = \{\mathbf{G}\mathbf{\Phi}, \mathbf{c}\} \subset \mathbb{R}^n$ is an RPI set of $\mathbf{x}(k+1) = \mathbf{A_K}\mathbf{x}(k) + \mathbf{w}(k)$ if $\mathbf{w}(k) \in \mathcal{W} = \{\mathbf{G}_w, \mathbf{c}_w\}$, and there exists $\mathbf{\Gamma}_1 \in \mathbb{R}^{n_g \times n_g}$, $\mathbf{\Gamma}_2 \in \mathbb{R}^{n_g \times n_w}$, and $\boldsymbol{\beta} \in \mathbb{R}^{n_g}$ such that

$$\mathbf{A_K}\mathbf{G}\mathbf{\Phi} = \mathbf{G}\mathbf{\Gamma}_1, \quad (15a)$$

$$\mathbf{G}_w = \mathbf{G}\mathbf{\Gamma}_2, \quad (15b)$$

$$(\mathbf{I} - \mathbf{A_K})\mathbf{c} - \mathbf{c}_w = \mathbf{G}\boldsymbol{\beta}, \quad (15c)$$

$$|\mathbf{\Gamma}_1|\mathbf{1} + |\mathbf{\Gamma}_2|\mathbf{1} + |\boldsymbol{\beta}| \leq \mathbf{\Phi}\mathbf{1}. \quad (15d)$$

Theorem 2 can be applied to determine the RPI set $\mathcal{Z}(\mathbf{\Phi})$ for a predetermined generator matrix $\mathbf{G}$. For a desired order of $\mathcal{Z}$, $\mathbf{G}$ can be determined using $\mathbf{G}_w$ and $\mathbf{A_K}$ as $\mathbf{G} = [\mathbf{G}_w \ \mathbf{A_K}\mathbf{G}_w \ \ldots \ \mathbf{A_K}^s\mathbf{G}_w]$, for some $s \in \mathbb{N}_+$ that provides the desired order. Thus $\mathbf{G}$ is a truncated version of the infinite sum used to compute the mRPI set in [13]. However, for an improper choice of $\mathbf{G}$ or with an inadequate number of generators in $\mathbf{G}$, there might not exist a $\mathbf{\Phi}$ that scales $\mathcal{Z}(\mathbf{\Phi})$ to satisfy (15), resulting in an infeasible optimization problem. Assuming a properly chosen $\mathbf{G}$, the size of $\mathcal{Z}$ can be scaled by the diagonal matrix $\mathbf{\Phi}$ such that $\mathcal{Z}(\mathbf{\Phi})$ is an approximation of the mRPI set, where $\mathbf{\Phi}$ is determined by solving an optimization problem with the constraints from (15) and an objective function that minimizes the scaling variables in $\mathbf{\Phi}$. This approach is an indirect attempt to minimize the volume of $\mathcal{Z}(\mathbf{\Phi})$, since directly optimizing the volume of a zonotope is a nonconvex problem [27]. With $\mathbf{c}$, $\mathbf{\Phi}$, $\mathbf{\Gamma}_1$, $\mathbf{\Gamma}_2$, and $\boldsymbol{\beta}$ as decision variables, (15) consists of only linear constraints and thus a LP or QP can be formulated based on the p-norm used to minimize the vector ϕ, where $\mathbf{\Phi} = \text{diag}(\phi)$.

Theorem 3: (Theorem 7 of [16]) Given $\mathcal{Z}_1 = \{\mathbf{G}_1, \mathbf{c}_1\}$ and $\mathcal{Z}_2 = \{\mathbf{G}_2, \mathbf{c}_2\}$, then $\tilde{\mathcal{Z}}_d = \{\mathbf{G}_d\mathbf{\Phi}, \mathbf{c}_d\}$, with $\mathbf{\Phi} = diag(\boldsymbol{\phi}), \phi_i > 0, \forall i \in \{1, \cdots, n_{g_d}\}$, is an inner-approximation of the Pontryagin difference $\mathcal{Z}_d = \mathcal{Z}_1 \ominus \mathcal{Z}_2$ such that $\tilde{\mathcal{Z}}_d \subseteq \mathcal{Z}_d$ if there exists $\mathbf{\Gamma} \in \mathbb{R}^{n_{g_1} \times (n_{g_d} + n_{g_2})}$ and $\boldsymbol{\beta} \in \mathbb{R}^{n_{g_1}}$ such that

$$\begin{bmatrix}\mathbf{G}_d\mathbf{\Phi} & \mathbf{G}_2\end{bmatrix} = \mathbf{G}_1\mathbf{\Gamma}, \quad (16a)$$

$$\mathbf{c}_1 - (\mathbf{c}_d + \mathbf{c}_2) = \mathbf{G}_1\boldsymbol{\beta}, \quad (16b)$$

$$|\mathbf{\Gamma}|\mathbf{1} + |\boldsymbol{\beta}| \leq \mathbf{1}. \quad (16c)$$

Theorem 3 can be applied to compute $\tilde{\mathcal{Z}}_d \subseteq \mathcal{Z}_d$ and it is practical to assume the generator matrix $\mathbf{G}_d$ is comprised of the generators from both $\mathcal{Z}_1$ and $\mathcal{Z}_2$ such that $\mathbf{G}_d = \begin{bmatrix}\mathbf{G}_1 & \mathbf{G}_2\end{bmatrix}$. The set $\tilde{\mathcal{Z}}_d$ with maximal volume is typically desired and can be computed by solving an optimization problem formulated with the constraints from (16) and an objective function that maximizes the scaling variables in $\mathbf{\Phi}$. With $\mathbf{c}_d$, $\mathbf{\Phi}$, $\mathbf{\Gamma}$, and $\boldsymbol{\beta}$ as decision variables in this optimization problem, (16) consists of only linear constraints and thus a LP or QP can be formulated based on the p-norm used to maximize the vector ϕ, where $\mathbf{\Phi} = \text{diag}(\phi)$.

VI. One-step RPI Set Computation and Constraint Tightening

When analyzing (11), the addition of scalable sets introduces the need to 1) enforce point containment within a scaled tightened constraint set (e.g. $\hat{\mathbf{x}}(j|k) \in \tilde{\mathcal{X}}(\mathbf{\Phi}_x)$) and 2) set containment for inner-approximations of the tightened constraint set (e.g. $\tilde{\mathcal{X}}(\mathbf{\Phi}_x) \oplus \tilde{\mathcal{E}}(\mathbf{\Phi}_\varepsilon) \subseteq \mathcal{X}$) and the outer-approximation of the mRPI set (e.g. $\mathbf{A_K}\tilde{\mathcal{E}}(\mathbf{\Phi}_\varepsilon) \oplus \mathcal{W}(\mathbf{\Phi}_w) \subseteq \tilde{\mathcal{E}}(\mathbf{\Phi}_\varepsilon)$). To reduce unnecessary complexity and highlight the ability to simultaneously formulate these containment conditions as linear constraints, the following optimization problem is introduced for some predefined point $\hat{\mathbf{x}}(j|k)$ and sets $\mathcal{X}$, $\tilde{\mathcal{X}}$, $\tilde{\mathcal{E}}$, and $\mathcal{W}$.

$$\min_{\mathbf{\Phi}_x, \mathbf{\Phi}_\varepsilon, \mathbf{\Phi}_w} \ell_{\mathbf{\Phi}}, \tag{17a}$$

s.t.

$$\hat{\mathbf{x}}(j|k) \in \tilde{\mathcal{X}}(\mathbf{\Phi}_x), \tag{17b}$$

$$\tilde{\mathcal{X}}(\mathbf{\Phi}_x) \oplus \tilde{\mathcal{E}}(\mathbf{\Phi}_\varepsilon) \subseteq \mathcal{X}, \tag{17c}$$

$$\mathbf{A_K}\tilde{\mathcal{E}}(\mathbf{\Phi}_\varepsilon) \oplus \mathcal{W}(\mathbf{\Phi}_w) \subseteq \tilde{\mathcal{E}}(\mathbf{\Phi}_\varepsilon). \tag{17d}$$

The following subsections use *Theorems 2* and *3* to convert the point and set containment conditions from (17b)-(17d) to linear constraints and discuss how to formulate the cost function in (17a) to optimize the size of these sets. Note that similar linear constraints and cost functions designs can be formulated for the input and terminal constraint sets conditions from (11d), (11g), and (11h) to recast all of the constraints in (11) as linear constraints.

A. Containment Constraints

Theorem 4: Given $\mathcal{X} = \{\mathbf{G}_x, \mathbf{c}_x\}$, let $\tilde{\mathcal{X}} = \{\tilde{\mathbf{G}}_x\mathbf{\Phi}_x, \tilde{\mathbf{c}}_x\}$ and $\tilde{\mathcal{E}} = \{\mathbf{G}_\varepsilon\mathbf{\Phi}_\varepsilon, \mathbf{c}_\varepsilon\}$. Then (17b)-(17d) are satisfied if there exists $\boldsymbol{\xi}_x \in \mathbb{R}^{n_x}, \mathbf{\Gamma}_1 \in \mathbb{R}^{n_x \times (n_{\tilde{x}}+n_\varepsilon)}$, $\boldsymbol{\beta}_1 \in \mathbb{R}^{n_x}, \mathbf{\Gamma}_2 \in \mathbb{R}^{n_\varepsilon \times n_\varepsilon}, \mathbf{\Gamma}_3 \in \mathbb{R}^{n_\varepsilon \times n_w}$, and $\boldsymbol{\beta}_2 \in \mathbb{R}^{n_\varepsilon}$ such that

$$\hat{\mathbf{x}}(j|k) = \tilde{\mathbf{G}}_x\boldsymbol{\xi}_x + \tilde{\mathbf{c}}_x, \quad -\mathbf{\Phi}_x \leq \boldsymbol{\xi}_x \leq \mathbf{\Phi}_x, \tag{18a}$$

$$\begin{bmatrix}\tilde{\mathbf{G}}_x\mathbf{\Phi}_x & \mathbf{G}_\varepsilon\mathbf{\Phi}_\varepsilon\end{bmatrix} = \mathbf{G}_x\mathbf{\Gamma}_1, \tag{18b}$$

$$\mathbf{c}_x - (\tilde{\mathbf{c}}_x + \mathbf{c}_\varepsilon) = \mathbf{G}_x\boldsymbol{\beta}_1, \tag{18c}$$

$$|\mathbf{\Gamma}_1|\mathbf{1} + |\boldsymbol{\beta}_1| \leq \mathbf{1}, \tag{18d}$$

$$\mathbf{A_K}\mathbf{G}_\varepsilon\mathbf{\Phi}_\varepsilon = \mathbf{G}_\varepsilon\mathbf{\Gamma}_2, \tag{18e}$$

$$\mathbf{G}_w = \mathbf{G}_\varepsilon\mathbf{\Gamma}_3, \tag{18f}$$

$$(\mathbf{I} - \mathbf{A_K})\mathbf{c}_\varepsilon - \mathbf{c}_w = \mathbf{G}_\varepsilon\boldsymbol{\beta}_2, \tag{18g}$$

$$|\mathbf{\Gamma}_2|\mathbf{1} + |\mathbf{\Gamma}_3|\mathbf{1} + |\boldsymbol{\beta}_2| \leq \mathbf{\Phi}_\varepsilon\mathbf{1}. \tag{18h}$$

Proof: The proof requires showing that (18a) enforces the point containment condition from (17b), (18b)-(18d) enforce the Pontryagin difference definition (17c), and (18e)-(18h) enforce the definition of an RPI set from (5). Consider the change of variables $\boldsymbol{\xi}_x = \mathbf{\Phi}_x\hat{\boldsymbol{\xi}}_x$, $\mathbf{\Gamma}_2 = \mathbf{\Phi}_\varepsilon\tilde{\mathbf{\Gamma}}_2$, $\mathbf{\Gamma}_3 = \mathbf{\Phi}_\varepsilon\tilde{\mathbf{\Gamma}}_3$, $\boldsymbol{\beta}_2 = \mathbf{\Phi}_\varepsilon\tilde{\boldsymbol{\beta}}_2$ and define $\tilde{\mathbf{\Gamma}}_{23} = \begin{bmatrix}\tilde{\mathbf{\Gamma}}_2 & \tilde{\mathbf{\Gamma}}_3\end{bmatrix}$. Then, (18a) readily satisfies the definition of a zonotope with $\hat{\boldsymbol{\xi}}_x \in [-\mathbf{1}, \mathbf{1}]$. The Pontryagin difference containment conditions from *Theorem 3* are satisfied by (18b)-(18d). Then the zonotope containment conditions from *Lemma 1* are satisfied by 1) rearranging and combining (18e) and (18f) to get $\begin{bmatrix}\mathbf{A_K}\mathbf{G}_\varepsilon\mathbf{\Phi}_\varepsilon & \mathbf{G}_w\end{bmatrix} = \mathbf{G}_\varepsilon\mathbf{\Phi}_\varepsilon\tilde{\mathbf{\Gamma}}_{23}$, 2) rearranging (18g) to get $\mathbf{c}_\varepsilon - (\mathbf{A_K}\mathbf{c}_\varepsilon + \mathbf{c}_w) = \mathbf{G}_\varepsilon\mathbf{\Phi}_\varepsilon\tilde{\boldsymbol{\beta}}_2$, and 3) multiplying (18h) by $\mathbf{\Phi}_\varepsilon^{-1}$, since $\phi_i > 0$, to get $|\tilde{\mathbf{\Gamma}}_{23}|\mathbf{1} + |\tilde{\boldsymbol{\beta}}_2| \leq \mathbf{1}$. ■

B. Cost Function

In determining the cost function $\ell_{\mathbf{\Phi}}$, it is typically desired to let $\ell_{\mathbf{\Phi}}$ be a linear or a quadratic function of $\mathbf{\Phi}_x, \mathbf{\Phi}_\varepsilon, \mathbf{\Phi}_w$ so that (17), and therefore (11), remains a linear or quadratic program. Conceptually, $\ell_{\mathbf{\Phi}}$ should be defined to maximize the size of the uncertainty set $\mathcal{W}(\mathbf{\Phi}_w)$ while minimizing the outer-approximation of the mRPI set $\tilde{\mathcal{E}}(\mathbf{\Phi}_\varepsilon)$ and maximizing the inner-approximation of the tightened constraint set $\tilde{\mathcal{X}}(\mathbf{\Phi}_x)$. Interestingly, maximizing $\tilde{\mathcal{X}}(\mathbf{\Phi}_x)$ automatically incentivizes minimizing $\tilde{\mathcal{E}}(\mathbf{\Phi}_\varepsilon)$. Thus, $\ell_{\mathbf{\Phi}}$ should be designed to maximize $\mathbf{\Phi}_w$ while also maximizing $\mathbf{\Phi}_x$. However, maximizing $\mathbf{\Phi}_x$ alone would minimize $\mathbf{\Phi}_w$, and vice-versa, and thus there is a trade-off.

With $\mathbf{\Phi}_w = diag(\phi_w)$ and $\mathbf{\Phi}_x = diag(\phi_x)$, one approach to formulating $\ell_{\mathbf{\Phi}}$ is based on the norms of the scaling variables such that

$$\ell_{\mathbf{\Phi}} = -\|\phi_x\|_p - \lambda\|\phi_w\|_p, \ \lambda \geq 0, \tag{19}$$

where the p-norms, $\|\cdot\|_p$, can be used to express the 1-norm, 2-norm, or ∞-norm. The weighting term λ can be used to tune the priority between maximizing the uncertainty and tightened constraint sets. Similar scaling variables have been used in [27] to outer-approximate asymmetric polytopes by scaled zonotopes obtained by maximizing the 1- and ∞-norm of the generators. However, maximizing the p-norm of the scaling variables may not effectively maximize the *volume* of these approximating sets, as will be shown in *Example 1*.

Alternatively, the Hausdorff distance can be used to effectively maximize the size of the tightened constraint set such that $\tilde{\mathcal{X}}(\mathbf{\Phi}_x)$ inner-approximates $\hat{\mathcal{X}}$. As defined in [17], the Hausdorff distance d for two sets $\mathcal{P}$ and $\mathcal{Q}$ is

$$d = \min_{0 \leq d \in \mathbb{R}} \{\mathcal{Q} \subseteq \mathcal{P} \oplus d\mathcal{B}, \quad \mathcal{P} \subseteq \mathcal{Q} \oplus d\mathcal{B}\}. \tag{20}$$

Using this Hausdorff distance metric, the optimization problem from (17) is modified as

$$\min_{d_x} \ell_d, \tag{21a}$$

s.t.

$$\mathcal{X} \subseteq \tilde{\mathcal{X}}(\mathbf{\Phi}_x) \oplus d_x\mathcal{B}, \tag{21b}$$

$$\hat{\mathbf{x}}(j|k) \in \tilde{\mathcal{X}}(\mathbf{\Phi}_x), \tag{21c}$$

$$\tilde{\mathcal{X}}(\mathbf{\Phi}_x) \oplus \tilde{\mathcal{E}}(\mathbf{\Phi}_\varepsilon) \subseteq \mathcal{X}, \tag{21d}$$

$$\mathbf{A_K}\tilde{\mathcal{E}}(\mathbf{\Phi}_\varepsilon) \oplus \mathcal{W}(\mathbf{\Phi}_w) \subseteq \tilde{\mathcal{E}}(\mathbf{\Phi}_\varepsilon). \tag{21e}$$

Theorem 5: Given $\mathcal{X} = \{\mathbf{G}_x, \mathbf{c}_x\}$ and $\tilde{\mathcal{X}} = \{\tilde{\mathbf{G}}_x\mathbf{\Phi}_x, \tilde{\mathbf{c}}_x\}$, the containment property in (21b) is satisfied if there exists $\mathbf{\Gamma}_4 \in \mathbb{R}^{n_{\tilde{x}} \times n_x}, \mathbf{\Gamma}_5 \in \mathbb{R}^{n \times n_x}$, $\boldsymbol{\beta}_3 \in \mathbb{R}^{n_{\tilde{x}}}, \boldsymbol{\beta}_4 \in \mathbb{R}^n$ such that

$$\mathbf{G}_x = \tilde{\mathbf{G}}_x\mathbf{\Gamma}_4 + \mathbf{\Gamma}_5, \tag{22a}$$

$$\tilde{\mathbf{c}}_x - \mathbf{c}_x = \tilde{\mathbf{G}}_x\boldsymbol{\beta}_3 + \boldsymbol{\beta}_4, \tag{22b}$$

$$|\mathbf{\Gamma}_4|\mathbf{1} + |\boldsymbol{\beta}_3| \leq \mathbf{\Phi}_x\mathbf{1}, \tag{22c}$$

$$|\mathbf{\Gamma}_5|\mathbf{1} + |\boldsymbol{\beta}_4| \leq d_x\mathbf{1}. \tag{22d}$$

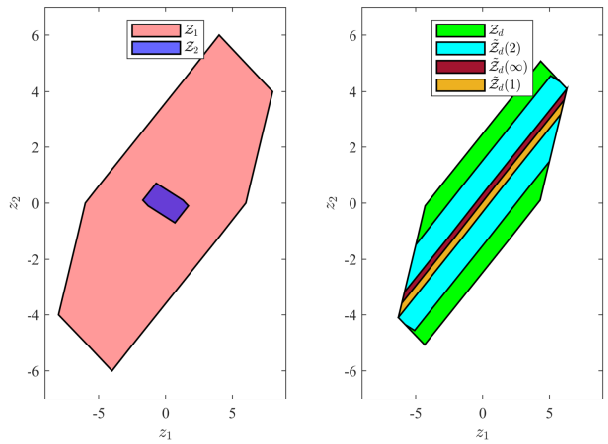

Fig. 1. Left: Given zonotopes $\mathcal{Z}_1, \mathcal{Z}_2$. Right: The Pontryagin difference $\mathcal{Z}_d$ is shown in green and the inner-approximating Pontryagin differences computed using *Theorem 3* for $p = 1, 2$, and ∞ are shown in yellow, cyan, and brown.

Proof: The proof requires using *Lemma 1* to show that (22a)-(22d) enforce the zonotope containment condition from (21b). Consider the change of variables $\mathbf{\Gamma_4} = \mathbf{\Phi}_x\tilde{\mathbf{\Gamma}}_4$, $\boldsymbol{\beta}_3 = \mathbf{\Phi}_x\tilde{\boldsymbol{\beta}}_3$, $\mathbf{\Gamma}_5 = d_x\tilde{\mathbf{\Gamma}}_5$, $\boldsymbol{\beta}_4 = d_x\tilde{\boldsymbol{\beta}}_4$, and let $\mathbf{\Gamma}_{45} = \begin{bmatrix}\mathbf{\Gamma}_4^\top & \mathbf{\Gamma}_5^\top\end{bmatrix}^\top$ and $\boldsymbol{\beta}_{34} = \begin{bmatrix}\boldsymbol{\beta}_3^\top & \boldsymbol{\beta}_4^\top\end{bmatrix}^\top$. Then the zonotope containment conditions from *Lemma 1* are readily satisfied by expressing (22a) in terms of $\mathbf{\Gamma}_{45}$ to get $\mathbf{G}_x = \begin{bmatrix}\tilde{\mathbf{G}}_x & \mathbf{I}\end{bmatrix}\mathbf{\Gamma}_{45}$ and expressing (22b) in terms of $\boldsymbol{\beta}_{34}$ to get $\tilde{\mathbf{c}}_x - \mathbf{c}_x = \begin{bmatrix}\tilde{\mathbf{G}}_x & \mathbf{I}\end{bmatrix}\boldsymbol{\beta}_{34}$. Then, (22c) is written in terms of $\tilde{\mathbf{\Gamma}}_4$ and $\tilde{\boldsymbol{\beta}}_3$ to get $|\mathbf{\Phi}_x\tilde{\mathbf{\Gamma}}_4|\mathbf{1} + |\mathbf{\Phi}_x\tilde{\boldsymbol{\beta}}_3| \leq \mathbf{\Phi}_x\mathbf{1}$, while (22d) is written in terms of $\tilde{\mathbf{\Gamma}}_5$ and $\tilde{\boldsymbol{\beta}}_4$ to get $|d_x\tilde{\mathbf{\Gamma}}_5|\mathbf{1} + |d_x\tilde{\boldsymbol{\beta}}_4| \leq d_x\mathbf{1}$. Cancelling $\mathbf{\Phi}_x$ and d_x in these equations results in $|\tilde{\mathbf{\Gamma}}_4|\mathbf{1} + |\tilde{\boldsymbol{\beta}}_3| \leq \mathbf{1}$ and $|\tilde{\mathbf{\Gamma}}_5|\mathbf{1} + |\tilde{\boldsymbol{\beta}}_4| \leq \mathbf{1}$. Finally, letting $\tilde{\mathbf{\Gamma}}_{45} = \begin{bmatrix}\tilde{\mathbf{\Gamma}}_4^\top & \tilde{\mathbf{\Gamma}}_5^\top\end{bmatrix}^\top$ and $\tilde{\boldsymbol{\beta}}_{34} = \begin{bmatrix}\tilde{\boldsymbol{\beta}}_3^\top & \tilde{\boldsymbol{\beta}}_4^\top\end{bmatrix}^\top$, these equations are concatenated vertically to obtain the final result $|\tilde{\mathbf{\Gamma}}_{45}|\mathbf{1} + |\tilde{\boldsymbol{\beta}}_{34}| \leq \mathbf{1}$. ■

The cost function in (21a) minimizes the Hausdorff distance between the state constraint set $\mathcal{X}$ and the inner-approximating tightened state constraint set $\tilde{\mathcal{X}}(\mathbf{\Phi}_x)$. Similar to (17a), minimizing the Hausdorff distance maximizes $\tilde{\mathcal{X}}(\mathbf{\Phi}_x)$ which incentivizes minimizing $\tilde{\mathcal{E}}(\mathbf{\Phi}_\varepsilon)$. The cost ℓ_d is formulated based on the Hausdorff distance d_x such that

$$\ell_d = d_x - \lambda||\phi_w||_p. \tag{23}$$

Similar to (19), the weighting term λ provides the desired tradeoff between maximizing the uncertainty and tightened constraint sets where increasing λ should increase the size of the uncertainty set. The following example demonstrates the performance of minimizing the Hausdorff distance metric over maximizing the norm of the scaling variables.

Example 1: Consider the zonotopes

$$\mathcal{Z}_1 = \left\{\begin{bmatrix}5 & 2 & 1\\ 3 & -1 & 2\end{bmatrix}, \begin{bmatrix}0\\0\end{bmatrix}\right\},\ \mathcal{Z}_2 = \left\{\begin{bmatrix}1 & 0.2 & 0.5\\ -0.3 & -0.1 & 0.3\end{bmatrix}, \begin{bmatrix}0\\0\end{bmatrix}\right\},$$

shown in the left subplot of Fig. 1. First, the Pontryagin difference $\mathcal{Z}_d = \mathcal{Z}_1 \ominus \mathcal{Z}_2$ is computed in H-Rep using the Multi-Parametric Toolbox [28] as a benchmark for volume ratio comparison, as shown in green in the right subplot. The inner-approximations of the Pontryagin difference $\tilde{\mathcal{Z}}_d \subseteq \mathcal{Z}_d$ computed using *Theorem 3* are shown in the right subplot for $p = 1, 2$, and ∞. The best approximation is obtained with $p = 2$ by solving a QP instead of a LP with $V_r = 0.80$. For $p = 1$ and ∞, the volume ratios are 0.29 and 0.38.

However, choosing to compute $\tilde{\mathcal{Z}}_d$ by minimizing the Hausdorff distance based cost function in (23) results in the exact set $\mathcal{Z}_d$ with $V_r = 1$ while still solving a LP. ■

Using *Theorems 4* and *5* along with the Hausdorff distance based cost function from (23), the tightened input and terminal state constraint set conditions in (11d), (11g) and (11h) can also be formulated as linear constraints. Thus, the sizes of the uncertainty set, state, input, and terminal constraint sets can all be simultaneously optimized online along with the nominal state and input trajectories enabling the proposed tube-based robust MPC framework. By optimizing $\mathbf{\Phi}_w$ at every update of the controller, the proposed approach provides the desired time-varying balance between flexibility and performance.

The following numerical example demonstrates the key features of the proposed approach.

VII. Numerical Example

A simplified vehicle system model is considered with

$$\mathbf{x}(k+1) = \begin{bmatrix}1 & 1\\ 0 & 1\end{bmatrix}\mathbf{x}(k) + \begin{bmatrix}0\\1\end{bmatrix}\mathbf{u}(k) + \begin{bmatrix}0\\1\end{bmatrix}\mathbf{w}(k), \tag{24}$$

where the states $\mathbf{x}(k) \in \mathbb{R}^2$ represent position and velocity, input $\mathbf{u}(k) \in \mathbb{R}^1$ represents acceleration/deceleration, and the uncertainty $\mathbf{w}(k) \in \mathcal{W}(\mathbf{\Phi}_w) = \{||\mathbf{w}(k)||_\infty \leq \mathbf{\Phi}_w\}, \mathbf{\Phi}_w \in \mathbb{R}$ affects only the velocity state. Note that the scaling matrix $\mathbf{\Phi}_w$ of the uncertainty set $\mathcal{W}(\mathbf{\Phi}_w) = \{\mathbf{G}_w\mathbf{\Phi}_w, \mathbf{c}_w\}$ is computed as part of the robust MPC optimization problem in (11) with $\mathbf{c}_w = 0$, and $\mathbf{G}_w = 1$. The system and controller have time step size $\Delta t = 1$ second. The prediction horizon is $N = 100$ steps.

Starting from an initial condition $\mathbf{x}(0) = [0\ 0]^\top$, the desired operation is defined by tracking references $\{\mathbf{r}(k)\}_{k=0}^N$ for the position state and the acceleration/deceleration input (as shown in Fig. 2) using the weighted quadratic cost function

$$\ell(\mathbf{x}(j), \mathbf{u}(j), \mathbf{r}(j)) = ||\mathbf{r}(j) - \mathbf{z}(j)||_{\mathbf{I}}^2, \tag{25}$$

where $\mathbf{z}(j) = \begin{bmatrix}[1\ 0]\mathbf{x}(j)\\ \mathbf{u}(j)\end{bmatrix}$. The state constraint set $\mathcal{X}$ and input constraint set $\mathcal{U}$ are defined as

$$\begin{bmatrix}-1\\-5\end{bmatrix} \leq \mathbf{x}(k) \leq \begin{bmatrix}60\\5\end{bmatrix}, \quad -0.5 \leq \mathbf{u}(k) \leq 0.5.$$

The position reference was intentionally designed to be on the boundary of $\mathcal{X}$ to clearly demonstrate the tradeoff between cost performance and uncertainty set optimization. The terminal set for the robust MPC is $\hat{\mathcal{T}} = \tilde{\mathcal{T}}(\mathbf{\Phi}_t) = [0\ 0]^\top$.

Different values of uncertainty weighting λ from (23) ranging from 10^1 to 5×10^7 are considered to analyze the relationship between the uncertainty scaling variable $\mathbf{\Phi}_w$, the corresponding RPI and tightened constraint sets, and

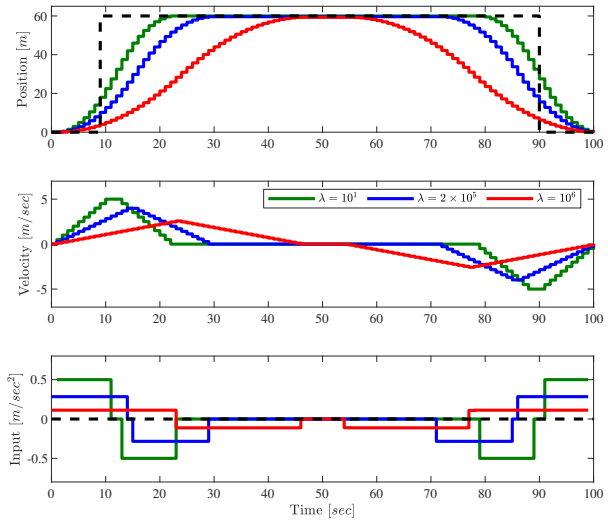

Fig. 2. Simulation results for uncertainty weightings $\lambda \in \{10^1, 2 \times 10^5, 10^6\}$ with the dashed lines denoting the reference trajectories for the position state and the acceleration/deceleration input.

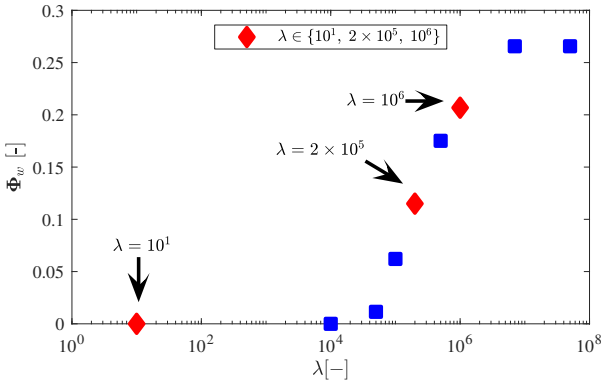

Fig. 3. Relationship between the chosen value of λ and the resulting uncertainty set size captured by $\mathbf{\Phi}_w$.

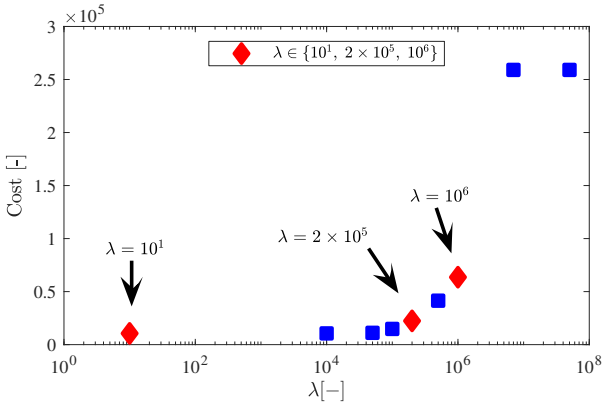

Fig. 4. Relationship between the chosen value of λ and the resulting operational cost computed using (25).

the vehicle performance. Fig. 3 shows the trend between λ and $\mathbf{\Phi}_w$ which determines the size of $\mathcal{W}$. Note that the uncertainty set size increases with λ. Similarly, Fig. 4 shows that the total operational cost based on (25) also increases with λ. For clarity of exposition, three key data points, corresponding to $\lambda \in \{10^1, 2 \times 10^5, 10^6\}$ were identified to more closely study the relationship between uncertainty set size and system operation.

Fig. 2 shows the simulation results using the proposed robust MPC for the chosen values of λ. The first subplot shows the reduction in position reference tracking performance corresponding to increasing values of λ. This reduced performance is a result of the reduced vehicle velocities shown in the second subplot and the reduced acceleration and deceleration shown in the third subplot. Specifically, the magnitude of the inputs decreases to compensate for the growing uncertainty set size. Intuitively, with increasing uncertainty set size, more of the control input is allocated to disturbance rejection, leaving less of the control input to be used for nominal acceleration and deceleration of the vehicle. Note that position reference tracking performance is also reduced under increasing uncertainty set size since the reference position of 60 m is no longer in the tightened state constraint set $\tilde{\mathcal{X}}$.

Fig. 5 shows the tightened state constraint set $\tilde{\mathcal{X}}(\mathbf{\Phi}_x)$ and tightened input constraint set $\tilde{\mathcal{U}}(\mathbf{\Phi}_u)$ from (10) for different uncertainty set sizes realized for the chosen values of λ. Clearly, the volume of the tightened state and input constraint sets decrease as the uncertainty set size increases.

An important limitation of the proposed approach is the conservatism introduced by the one-step approximation of the RPI set and corresponding constraint tightening. As shown in Fig. 6, $\tilde{\mathcal{E}}(\mathbf{\Phi}_\varepsilon)$ computed by solving (11) is an outer-approximation of the mRPI set $\mathcal{E}$ computed using the iterative approach from [13]. For both $\lambda \in \{2 \times 10^5, 10^6\}$, the volume ratio of $\tilde{\mathcal{E}}(\mathbf{\Phi}_\varepsilon)$ compared to $\mathcal{E}$ is $V_r = 1.26$. Additionally, the tightened state and input constraint sets are inner-approximations of $\hat{\mathcal{X}}$ and $\hat{\mathcal{U}}$ from (3c) and (3d) computed directly using the Pontryagin difference. For $\lambda \in \{2 \times 10^5, 10^6\}$, the volume ratios of $\tilde{\mathcal{X}}(\mathbf{\Phi}_x)$ compared to $\hat{\mathcal{X}}$ are $V_r = 0.99$ and $V_r = 0.987$ while the volume ratios of $\tilde{\mathcal{U}}(\mathbf{\Phi}_u)$ compared to $\hat{\mathcal{U}}$ are $V_r = 0.94$ and $V_r = 0.78$.

Using Yalmip [29] and Gurobi [30] to formulate and solve (11), the mean and maximum computation times are 0.26 and 0.42 seconds over 100 runs on a laptop with a 2.2 GHz i5 processor with 8 GB of RAM. By comparison, solving (3) has a mean and maximum computation times of 0.09 and 0.34 seconds with an additional 1.19 seconds required for the offline computation of RPI sets and corresponding constraint tightening. While including the uncertainty set size as a decision variable clearly increases the computation time, the proposed approach is expected to remain computationally viable for systems with significantly more states and inputs.

VIII. CONCLUSIONS

A tube-based robust MPC formulation with integrated set computation is presented for constrained linear systems. The size of the uncertainty set is computed online in the underlying control optimization problem. One-step RPI set and Pontryagin difference methods formulated based on

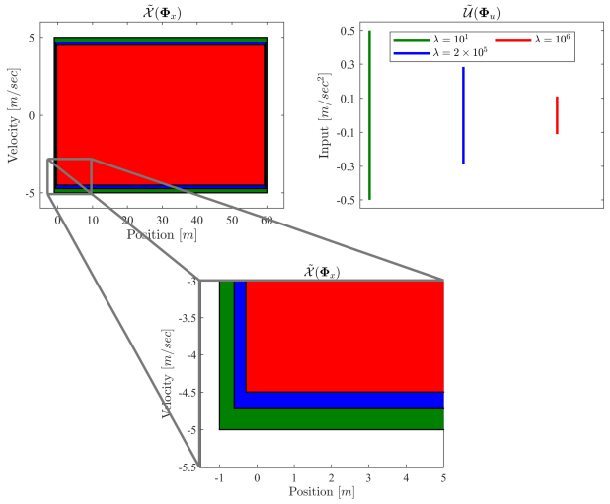

Fig. 5. Tightened state and input constraint sets implicitly showing the effect of the increasing uncertainty set size for $\lambda \in \{10^1, 2 \times 10^5, 10^6\}$.

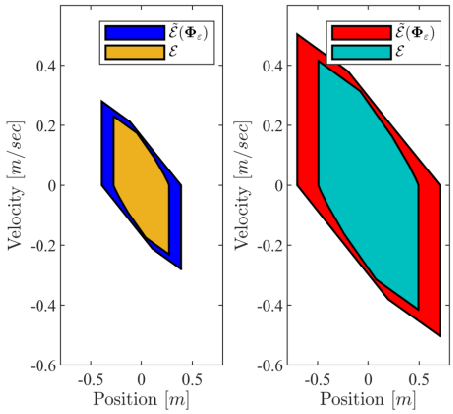

Fig. 6. Comparison of $\tilde{\mathcal{E}}(\mathbf{\Phi}_\varepsilon)$ and mRPI set $\mathcal{E}$ for $\lambda \in \{2 \times 10^5, 10^6\}$.

zonotopes and Hausdorff distance enabled online computation of RPI sets and tightened state and input constraint sets. A numerical example demonstrated the performance of the proposed tube-based robust MPC formulation and highlighted the benefits and limitations of embedding set calculations in the optimization problem. Future work will focus on the extension of the proposed tube-based robust MPC formulation to hierarchical MPC for online computation of disturbances between subsystems and between control decision at each level of the hierarchy.

REFERENCES

[1] D. Q. Mayne, J. B. Rawlings, C. V. Rao, and P. O.M. Scokaert. Constrained model predictive control: Stability and optimality. *Automatica*, 36:789–814, 2000.

[2] A. Bemporad and M. Morari. Robustness in identification and control. *Lecture Notes in Control and Information Sciences*, pages 207–226, 1999.

[3] W. Langson, I. Chryssochoos, S. V. Raković, and D. Q. Mayne. Robust model predictive control using tubes. *Automatica*, 40:125–133, 2004.

[4] D.Q. Mayne, M.M. Seron, and S.V. Raković. Robust Model Predictive Control of Constrained Linear Systems with Bounded Disturbances. *Automatica*, 41:219–224, 2005.

[5] Xiaojing Zhang, Maryam Kamgarpour, Angelos Georghiou, Paul Goulart, and John Lygeros. Robust optimal control with adjustable uncertainty sets. *Automatica*, 75:249–259, 2017.

[6] Yeojun Kim, Xiaojing Zhang, Jacopo Guanetti, and Francesco Borrelli. Robust Model Predictive Control with Adjustable Uncertainty Sets. *Conference on Decision and Control*, pages 5176–5181, 2019.

[7] X. Zhang, M. Kamgarpour, P. Goulart, and J. Lygeros. Selling robustness margins: A framework for optimizing reserve capacities for linear systems. *Conference on Decision and Control*, pages 6419–6424, 2014.

[8] Evangelos Vrettos, Frauke Oldewurtel, Fengtian Zhu, and Goran Andersson. Robust provision of frequency reserves by office building aggregations. *IFAC Proceedings*, 47:12068–12073, 2014.

[9] Tomasz T. Gorecki, Altug Bitlislioglu, Giorgos Stathopoulos, and Colin N. Jones. Guaranteeing input tracking for constrained systems: theory and application to demand response. *American Control Conference*, pages 232–237, 2015.

[10] Paul A. Trodden and J. M. Maestre. Distributed predictive control with minimization of mutual disturbances. *Automatica*, 77:31–43, 2017.

[11] Justin P. Koeln, Vignesh Raghuraman, and Brandon M. Hencey. Vertical hierarchical MPC for constrained linear systems. *Automatica*, 113:108817, 2020.

[12] Alberto Bemporad, Francesco Borrelli, and Manfred Morari. Min-Max Control of Constrained Uncertain Discrete-Time Linear Systems. *IEEE Transactions on Automatic Control*, 48(9):1600–1606, 2003.

[13] Sasa V. Raković, Eric C. Kerrigan, K. I. Kouramas, and D. Q. Mayne. Invariant approximations of the minimal robust positively invariant set. *IEEE Transactions on Automatic Control*, 50(3):406–410, 2005.

[14] Ilya Kolmanovsky and Elmer G. Gilbert. Theory and computation of disturbance invariant sets for discrete-time linear systems. *Mathematical Problems in Engineering*, 4(4):317–367, 1998.

[15] Paul Trodden. A One-Step Approach to Computing a Polytopic Robust Positively Invariant Set. *IEEE Transactions on Automatic Control*, 61(12):4100–4105, 2016.

[16] Vignesh Raghuraman and Justin P. Koeln. Set operations and order reductions for constrained zonotopes. *arXiv:2009.06039v1*, 2020.

[17] Sadra Sadraddini and Russ Tedrake. Linear Encodings for Polytope Containment Problems. *Conference on Decision and Control*, pages 4367–4372, 2019.

[18] Moritz Schulze Darup, Rainer Schaich, and Mark Cannon. How scaling of the disturbance set affects robust positively invariant sets for linear systems. *International Journal of Robust and Nonlinear Control*, 27(16):3236–3258, 2017.

[19] J. Koeln, H. Pangborn, M. Williams, M. Kawamura, and A. Alleyne. Hierarchical Control of Aircraft Electro-Thermal Systems. *IEEE Transactions on Control Systems Technology*, 28(4):1218–1232, 2020.

[20] L.J. Guibas, A. Nguyen, and L. Zhang. Zonotopes as bounding volumes. *SODA*, 3:803–812, 2003.

[21] Antoine Girard. Reachability of uncertain linear systems using zonotopes. In Manfred Morari and L. Thiele, editors, *Hybrid Systems: Computation and Control*, pages 291–305. Springer, 2005.

[22] Oded Maler. Computing reachable sets: an introduction. *Tech. Rep. French National Center of Scientific Research*, pages 1–8, 2008.

[23] M. Althoff, O. Stursberg, and M. Buss. Computing reachable sets of hybrid systems using a combination of zonotopes and polytopes. *Nonlinear Analysis: Hybrid Systems*, 4(2):233–249, 2010.

[24] Joseph K. Scott, Davide M. Raimondo, Giuseppe Roberto Marseglia, and Richard D. Braatz. Constrained zonotopes: A new tool for set-based estimation and fault detection. *Automatica*, 69:126–136, 2016.

[25] J. M. Bravo, T. Alamo, and E. F. Camacho. Robust MPC of constrained discrete-time nonlinear systems based on approximated reachable sets. *Automatica*, 42(10):1745–1751, 2006.

[26] Francesco Scibilia, Sorin Olaru, and Morten Hovd. On feasible sets for MPC and their approximations. *Automatica*, 47:133–139, 2011.

[27] D. Ioan, I. Prodan, F. Stoican, S. Olaru, and S.I. Niculescu. Complexity bounds for obstacle avoidance within a zonotopic framework. *American Control Conference*, pages 235–240, 2019.

[28] Martin Herceg, Michal Kvasnica, Colin N Jones, and Manfred Morari. Multi-parametric Toolbox 3.0. *European Control Conference*, pages 502–510, 2013.

[29] Johan Löfberg. YALMIP: A toolbox for modeling and optimization in MATLAB. *IEEE International Conference on robotics and automation*, pages 284–289, 2004.

[30] Gurobi Optimization Inc. Gurobi Optimizer Reference Manual. *www.gurobi.com*, 2019.